TOWARDS A NON-INVASIVE CANCER TREATMENT BY ELECTROMAGNETIC HYPERTHERMIA THERAPY

R. MATTOSO, A.A. NOVOTNY, AND R. PRAKASH

Abstract. This work is dedicated to pointwise antennas design for hyperthermia treatment. In particular, we want to find the optimal values of current densities passing through each antenna to selectively heat a specified target. The forward problem is governed by the steady-state heat equation in living tissues, which is coupled with the Maxwell's equations modeling the electromagnetism phenomenon. An objective functional measuring the difference between the target temperature and the temperature predicted by the model problem is minimized with respect to the current densities by using the topological derivative method. The resulting sensitivities are used to devise an antenna design algorithm. Finally, some numerical experiments are presented showing different features of the proposed methodology, including its capability in heating selectively a specific target by using only the natural material properties of the tissues without the help of artificial contrast agents, which potentially results in a fully noninvasive treatment.

1. Introdution

Disordered cell growth, usually called cancer, is a common disease that affects the entire world population and can develop in any part of the human body. According to World Health Organization's data painel of 2022 [23], there were almost 20 milion new cases and about 9.8 milion deaths worldwide in 2022. This same study points out that breast cancer ranks second in newly diagnosed cases and is also the forth more fatal kind of cancer. The observed increasing in the number of cancer cases is related to many factors, including population growth and its aging, economic development, and dietary patterns [5]. In some situations, there is a possibility of preventing the onset of cancer. For example, lung cancer is the leader in newly diagnosed cases, which in most of the time is a consequence of cigarette addiction or secondhand smoking [22].

Cancer prevention, treatment, and cure are extensively studied and discussed topics. The work by Debela et al. [3] highlights prospects for new approaches and procedures in this field. At the moment, the most common treatments for cancer are surgery, chemotherapy, radiotherapy, bone marrow transplantation, and also hyperthermia that can be used alone or combined with other treatments [25]. Chemotherapy and radiotherapy, when combined with hyperthermia therapy, become more effective allowing to be administered in lower doses. Hyperthermia consists in heating the tumor to a certain temperature to improve tumour oxygenation [4], usually between 40°C and 46°C [6, 15]. The heating of cells – both healthy and diseased – may cause their death, so that it is important to selectively heat the tumor for preventing the death of healthy cells [10]. This is in fact the main challenge in hyperthermia therapy, which has motivated many recent studies [8, 11, 21].

Regrading the literature, the paper [2] deals with topology design of electromagnetic distributed antennas. A gradient type method has been proposed, which successfully

Date: December 19, 2024.
Key words and phrases. Hyperthermia Therapy, Non-Invasive Treatment, Bioheat Equation, Maxwell Equation, Coupled System, Topological Derivative Method.

heat a single target per once. In contrast with [2], a novel approach for pointwise antennas design in hyperthermia treatment that selectively heat several targets simultaneously up to the desired temperature is proposed in [13]. Both works [2] and [13] consider an idealized scenario into two spatial dimensions. In this article, we present the three dimensional counterpart of [13], in which the electromagnetic phenomenon is governed by the Maxwell's equations and the antennas are represented by dipoles. More precisely, we want to find the optimal values of current densities passing through each antenna to selectively heat a specified target. The forward problem is governed by the steady-state heat equation in living tissues, which is coupled with the Maxwell's equations modeling the electromagnetism phenomenon. An objective functional measuring the difference between the target temperature and the temperature predicted by the model problem is minimized with respect to the current densities by using the topological derivative method. The resulting sensitivities are used to devise an antenna design algorithm. Finally, some numerical experiments are presented showing different features of the proposed methodology, including its capability in heating selectively a specific target by using only the natural material properties of the tissues without the help of artificial contrast agents [18, 19, 20], which potentially leads to a fully noninvasive treatment.

The organization of the paper is as follows: Section 2 outlines the mathematical formulation of the topology optimization problem under consideration. In Section 3, we introduce the topological sensitivity analysis and provide a computation of the cost function's variation due to small corresponding perturbations. In Section 4, we devise an algorithm for reconstruction using first order topological derivative. Finally, Section 5 offers extensive numerical examples showcasing the effectiveness of the proposed optimization algorithm, followed by a brief conclusion in 6.

2. Problem Setting

Let us consider an open and bounded domain $\mathcal{D} \subset \mathbb{R}^3$ with Lipschitz boundary $\partial\mathcal{D}$, where domain $\mathcal{D}$ is constituted by Ω surrounded by a Perfectly Matched Layer - PML. Let $\mathcal{B} \subset \Omega$ and $\mathcal{T} \subset \mathcal{B}$ represent the body healthy tissue and the target to be burned, respectively. The pointwise antennas are represented by the gradient of Dirac masses and belong to the set of admissible solutions $C_\delta(\Omega)$, which will be defined later on. See sketch in Figure 1.

Let the objective functional be defined as

$$\mathcal{J}(\Theta) = \beta_1 \int_{\mathcal{B}\setminus\mathcal{T}} (\Theta - \Theta_b)^2 \,\mathrm{d}\mathbf{x} + \beta_2 \int_{\mathcal{T}} (\Theta - \Theta^*)^2 \,\mathrm{d}\mathbf{x} \tag{2.1}$$

where $\Theta^* : \Omega \mapsto \mathbb{R}$ and $\Theta_b : \Omega \mapsto \mathbb{R}$ are the target and the blood temperatures, respectively. The weights $\beta_1 = \frac{1-\beta}{|\mathcal{B}\setminus\mathcal{T}|}$ and $\beta_2 = \frac{\beta}{|\mathcal{T}|}$, with $\beta \in (0,1)$. Finally, $\Theta : \Omega \mapsto \mathbb{R}$ is the body temperature function, solution to the following steady-state heat problem for *in-vivo* tissues [17, 24]:

$$\Theta \in \mathcal{O} : \int_\Omega \left[K\nabla\Theta \cdot \nabla\eta + c_b w(\Theta - \Theta_b)\eta\right] \mathrm{d}\mathbf{x} = \frac{1}{2}\int_\Omega \sigma \|E\|^2 \eta \,\mathrm{d}\mathbf{x}, \quad \forall \eta \in \mathcal{O}_0, \tag{2.2}$$

where $K : \Omega \mapsto \mathbb{R}$ is the thermal conductivity of the tissue [W m^{-1} K^{-1}], $c_b : \Omega \mapsto \mathbb{R}$ is the specific heat of the blood [J kg^{-1} K^{-1}], $w : \Omega \mapsto \mathbb{R}$ is the blood perfusion rate [kg m^{-3} s^{-1}] and $\sigma : \Omega \mapsto \mathbb{R}$ is the electrical conductivity of the medium [S m^{-1}]. The spaces function $\mathcal{O}$ and $\mathcal{O}_0$ are defined as

$$\mathcal{O} := \{\phi \in H^1(\Omega) : \phi_{|_{\partial\Omega}} = \Theta_\Gamma\} \quad \text{and} \quad \mathcal{O}_0 := H_0^1(\Omega), \tag{2.3}$$

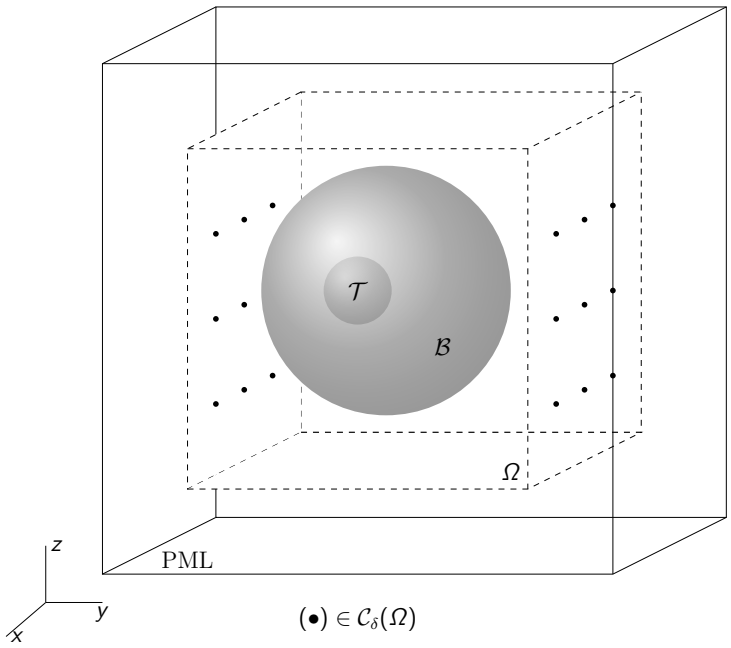

FIGURE 1. Problem region. The bigger cube represents the PML, the dashed cube is the Domain Ω, the bigger circle represents the body $\mathcal{B}$ and the small one represents the tumor $\mathcal{T}$. The dots in xz plane represent the poitwise antennas.

where Θ_Γ is a prescribed temperature on the boundary $\partial\Omega$. In addition, $E : \mathcal{D} \mapsto \mathbb{C}^d$ is solution to the Maxwell equations, namely

$$E \in \mathcal{W} : \int_{\mathcal{D}} \left[\nabla \times E \cdot \nabla \times W - \varepsilon\mu\omega^2 E \cdot W\right] \mathrm{d}\mathbf{x} = \int_{\mathcal{D}} Q \cdot W \, \mathrm{d}\mathbf{x}, \quad \forall W \in \mathcal{W}, \tag{2.4}$$

where ω is the angular frequency [rad s^{-1}], $\varepsilon = \varepsilon_r\varepsilon_0$ is the electrical permittivity [F m^{-1}], $\mu = \mu_r\mu_0$ is the magnetic permeability [H m^{-1}]. The quantities ε_r and μ_r are the relative electrical permittivity and magnetic permeability, respectively, whereas $\varepsilon_0 = 8.854\times10^{-12}$ F m^{-1} is the electrical permittivity and $\mu_0 = 4\pi\times10^{-7}$ H m^{-1} is the magnetic permeability, both associated with the free space. The functional space $\mathcal{W}$ is defined as

$$\mathcal{W} := \left\{\Phi \in H^1_{\mathrm{curl}}(\mathcal{D}) : \nu \times \Phi = 0 \text{ on } \partial\mathcal{D}\right\}, \tag{2.5}$$

where $H^1_{\mathrm{curl}}(\mathcal{D})$ is a complex valued Sobolev space, such that $\Phi \in L^2(\mathcal{D})$ and $\nabla \times \Phi \in L^2(\mathcal{D})$. Finally, $Q \in C_\delta(\Omega)$ is the source term representing the pointwise antennas, with

$$C_\delta(\Omega) = \left\{ Q \in L^2(\Omega) : Q(\mathbf{x}) = \sum_{i=1}^{N} q_i \nabla_{\mathbf{x}_i} \delta_\epsilon(\mathbf{x} - \mathbf{x}_i) \right\}, \tag{2.6}$$

where we are using a Gaussian function to approximate the dipoles, namely

$$\delta_\epsilon(\mathbf{x} - \mathbf{x}_i) = \frac{1}{\epsilon^3} \exp \frac{-\|\mathbf{x} - \mathbf{x}_i\|^2}{2\epsilon^2}, \tag{2.7}$$

in which $\epsilon > 0$ represents the aperture of the Gaussian function. The position of each antenna is represented by $\mathbf{x}_i \in \Omega \setminus \overline{\mathcal{B}}$, $i = 1, \cdots, N$, with N denoting the number of antennas. Finally, the quantity $q_i \in \mathbb{R}$ is the electric dipole intensity [C m^{-3}] and it is fixed in the coordinate (x_i, y_i, z_i). The ith-dipole is characterized by the term $\nabla_{\mathbf{x}_i}\delta_\epsilon(\mathbf{x}-\mathbf{x}_i)$ from (2.6), which represents electrostatic forces at the point $\mathbf{x}_i$ acting in opposite directions.

In fact, for ϵ small enough, each dipole has null-mean property in the sense that

$$\int_{\mathcal{D}} \nabla_{\mathbf{x}_i} \delta_\epsilon(\mathbf{x}-\mathbf{x}_i) d\mathbf{x} = \mathbf{0}, \tag{2.8}$$

which ensures charge conservation in the whole system. See the book by Aki and Richards [1, Ch. 3]. Physically, each dipole spreads the current q_i in all directions, allowing to heat the body $\mathcal{B}$ according to (2.2) and (2.4). From the above elements, the constrained optimization problem we are dealing with can be stated as following:

$$\underset{Q\in C_\delta(\Omega)}{\text{Minimize}}\ \mathcal{J}(\Theta), \quad \text{subject to (2.2) and (2.4).} \tag{2.9}$$

In order to simplify further analysis, we introduce two adjoint problems which are coupled in a reverse sense. The adjoint heat equation is written as: Find $\varphi \in \mathcal{O}_0$ such that

$$\int_\Omega [K\nabla\eta\cdot\nabla\varphi + c_b w\varphi\eta]\,\mathrm{d}\mathbf{x} = 2\beta_1 \int_{\mathcal{B}\setminus\mathcal{T}} (\Theta_b-\Theta)\eta\,\mathrm{d}\mathbf{x} + 2\beta_2 \int_{\mathcal{T}} (\Theta^*-\Theta)\eta\,\mathrm{d}\mathbf{x}, \quad \forall\eta\in\mathcal{O}_0, \tag{2.10}$$

and the Maxwell adjoint equation: Find $V \in \mathcal{W}$ such that

$$\int_{\mathcal{D}} \left[\nabla\times V\cdot\nabla\times W - \varepsilon\mu\omega^2 V\cdot W\right]\mathrm{d}\mathbf{x} = \int_\Omega \sigma\varphi\overline{E}\cdot W\,\mathrm{d}\mathbf{x}, \quad \forall W\in\mathcal{W}. \tag{2.11}$$

3. Topological Derivative Method

Following the Topological Derivative theory, let us now introduce a perturbation into the source Q, as

$$Q_\delta(\mathbf{x}) = Q(\mathbf{x}) + \sum_{i=N+1}^{M} q_i \nabla_{\mathbf{x}_i}\delta_\epsilon(\mathbf{x}-\mathbf{x}_i), \tag{3.1}$$

where $M > N$. Thus, the perturbed counterpart of the objective functional (2.1) is given by

$$\mathcal{J}(\Theta_\delta) = \beta_1 \int_{\mathcal{B}\setminus\mathcal{T}} (\Theta_\delta-\Theta_b)^2\,\mathrm{d}\mathbf{x} + \beta_2 \int_{\mathcal{T}} (\Theta_\delta-\Theta^*)^2\,\mathrm{d}\mathbf{x}, \tag{3.2}$$

where Θ_δ is solution to the perturbed heat problem

$$\Theta\in\mathcal{O}: \int_\Omega [K\nabla\Theta_\delta\cdot\nabla\eta + c_b w(\Theta_\delta-\Theta_b)\eta]\,\mathrm{d}\mathbf{x} = \frac{1}{2}\int_\Omega \sigma\|E_\delta\|^2\eta\,\mathrm{d}\mathbf{x}, \quad \forall\eta\in\mathcal{O}_0, \tag{3.3}$$

where E_δ is solution to the perturbed Maxwell problem

$$E_\delta\in\mathcal{W}: \int_{\mathcal{D}} \left[\nabla\times E_\delta\cdot\nabla\times W - \varepsilon\mu\omega^2 E_\delta\cdot W\right]\mathrm{d}\mathbf{x} = \int_{\mathcal{D}} Q_\delta\cdot W\,\mathrm{d}\mathbf{x}, \quad \forall W\in\mathcal{W}. \tag{3.4}$$

Let us consider the following *ansätze*

$$E_\delta = E + \sum_{i=N+1}^{M} q_i E_i, \tag{3.5}$$

$$\Theta_\delta = \Theta + \sum_{i=N+1}^{M} q_i\Theta_i + \sum_{i,j=N+1}^{M} q_i q_j \Theta_{ij}. \tag{3.6}$$

By replacing the *ansatz* (3.5) into (3.4), we obtain the set of Maxwell canonical problems given as:

$$E_i\in\mathcal{W}: \int_{\mathcal{D}} \left[\nabla\times E_i\cdot\nabla\times W - \varepsilon\mu\omega^2 E_i\cdot W\right]\mathrm{d}\mathbf{x} = \int_{\mathcal{D}} \nabla_{\mathbf{x}_i}\delta_\epsilon(\mathbf{x}-\mathbf{x}_i)\cdot W\,\mathrm{d}\mathbf{x}, \quad \forall W\in\mathcal{W}. \tag{3.7}$$

Analogously, after replacing (3.6) into (3.3), we obtain the set of heat canonical problems given by

$$\Theta_i \in \mathcal{O}_0 : \int_\Omega [K\nabla\Theta_i \cdot \nabla\eta + c_b w\Theta_i\eta]\,\mathrm{d}\mathbf{x} = \int_\Omega \sigma \mathrm{Re}\{E \cdot \bar{E}_i\}\eta\,\mathrm{d}\mathbf{x}, \quad \forall\eta \in \mathcal{O}_0, \tag{3.8}$$

for $i = N+1, \cdots, M$, and

$$\Theta_{ij} \in \mathcal{O}_0 : \int_\Omega [K\nabla\Theta_{ij} \cdot \nabla\eta + c_b w\Theta_{ij}\eta]\,\mathrm{d}\mathbf{x} = \frac{1}{2}\int_\Omega \sigma E_i \cdot \bar{E}_j\eta\,\mathrm{d}\mathbf{x}, \forall\eta \in \mathcal{O}_0, \tag{3.9}$$

for $i, j = N+1, \cdots, M$.

Finally, let us replace the *ansatz* (3.6) into the perturbed objective function (3.2) to obtain

$$\begin{aligned}
\mathcal{J}(\Theta_\delta) - \mathcal{J}(\Theta) = \beta_2 \int_{\mathcal{T}} \Big[& 2(\Theta - \Theta^*) \sum_{i=N+1}^{M} q_i\Theta_i + 2(\Theta - \Theta^*) \sum_{i,j=N+1}^{M} q_i q_j \Theta_{ij} \\
& + \sum_{i,j=N+1}^{M} q_i q_j \Theta_i \Theta_j + 2 \sum_{i,j,k=N+1}^{M} q_i q_j q_k \Theta_{ij}\Theta_k + \sum_{i,j,k,l=N+1}^{M} q_i q_j q_k q_l \Theta_{ij}\Theta_{kl} \Big]\,\mathrm{d}\mathbf{x} \\
& + \beta_1 \int_{\mathcal{B}\setminus\mathcal{T}} \Big[2(\Theta - \Theta_b) \sum_{i=N+1}^{M} q_i\Theta_i + 2(\Theta - \Theta_b) \sum_{i,j=N+1}^{M} q_i q_j \Theta_{ij} \\
& + \sum_{i,j=N+1}^{M} q_i q_j \Theta_i \Theta_j + 2 \sum_{i,j,k=N+1}^{M} q_i q_j q_k \Theta_{ij}\Theta_k + \sum_{i,j,k,l=N+1}^{M} q_i q_j q_k q_l \Theta_{ij}\Theta_{kl} \Big]\,\mathrm{d}\mathbf{x}.
\end{aligned} \tag{3.10}$$

The quantity (3.10) represents the exact sensitivity of the objective functional with respect to the introduction of a number $M - N$ additional pointwise antennas. In particular, we can recognize first, second, third and fourth orders derivatives associated with the terms multiplied by q_i, q_iq_j, $q_iq_jq_k$ and $q_iq_jq_kq_l$, respectively.

Remark 1. *It is interesting to observe that we obtain a finite expansion for the complete sensitive analysis even though the optimization problem* (2.9) *arises from a coupled system of two partial differential equations of different character. Actually, formula* (3.10) *has scope to devise a family of first to fourth order algorithms. In particular, we use it to produce a first order algorithm in Section 4 and numerical computations in Section 5. It will be interesting for the reader to see [16, Ch. 9, Sec. 9.2.3], for instance, where the authors had to settle for infinite series for perturbed objective functional and opt for asymptotic analysis.*

The sensitivity (3.10) can be used to devise reconstruction algorithms which find the optimal locations $\mathbf{x}_i^\star$ for the antennas as well as their optimal currents $q_i^\star$, similarly to proposed in [12]. However, we assume that the locations $\mathbf{x}_i$ are given and the optimal currents $q_i^\star$ have to be found, which allows to drop the summations in (3.10) from $1, \cdots, N$. Even in this scenario, the use of the sensitivity formula (3.10) still requires further simplification. Actually, the computation of all terms in (3.10) becomes unfeasible due to the combinatorial nature of problems for Θ_{ij} from (3.9). Therefore, our strategy is to truncate (3.10) up to the first order term. In particular, the following quantity is introduced:

$$\Psi(q_1, q_2, ..., q_N) = \beta_2 \int_{\mathcal{T}} 2(\Theta - \Theta^*) \sum_{i=N+1}^{M} q_i\Theta_i\,\mathrm{d}\mathbf{x} + \beta_1 \int_{\mathcal{B}\setminus\mathcal{T}} 2(\Theta - \Theta_b) \sum_{i=N+1}^{M} q_i\Theta_i\,\mathrm{d}\mathbf{x}, \tag{3.11}$$

where the summation is now defined from $i = 1$ up to N, with N used to denote a given number of antennas. Equation (3.11) can be conveniently written in a compact form as

$$\Psi(\mathbf{q}) = \mathbf{d} \cdot \mathbf{q}, \tag{3.12}$$

where $\mathbf{q} = (q_1, q_2, ..., q_N)^\top$, $\mathbf{d} = (d_1, d_2, ..., d_N)^\top$ is the first order derivative with entries

$$d_i = 2\beta_2 \int_{\mathcal{T}} (\Theta - \Theta^*)\Theta_i \, \mathrm{d}\mathbf{x} + 2\beta_1 \int_{\mathcal{B}\setminus\mathcal{T}} (\Theta - \Theta_b)\Theta_i \, \mathrm{d}\mathbf{x}, \tag{3.13}$$

with Θ solution to the heat problem (2.2) and Θ_i solutions to the variational problems (3.8).

4. Antenna Design Algorithms

In this section, we present a first order method for solving the optimization problem (2.9) with help of (3.12). In order to evaluate (3.12) the canonical problems (3.7) and (3.8) have to be solved for each point $\mathbf{x}_i$, $i = 1, \cdots, N$. Instead, we employ the adjoint sensitivity method, which simplifies such computations. In this context, we refer to the previously mentioned adjoint equations for heat and Maxwell equations. Actually, by setting $\eta = \varphi$ in (3.8) and $\eta = \Theta_i$ in (2.10), we obtain

$$\int_\Omega [K\nabla\Theta_i \cdot \nabla\varphi + c_b w \Theta_i \varphi] \, \mathrm{d}\mathbf{x} = \int_\Omega \sigma\varphi \mathrm{Re}\{E \cdot \overline{E}_i\} \, \mathrm{d}\mathbf{x}, \tag{4.1}$$

$$\int_\Omega [K\nabla\varphi \cdot \nabla\Theta_i + c_b w \varphi \Theta_i] \, \mathrm{d}\mathbf{x} = 2\beta_2 \int_{\mathcal{T}} (\Theta^* - \Theta)\Theta_i \, \mathrm{d}\mathbf{x} + 2\beta_1 \int_{\mathcal{B}\setminus\mathcal{T}} (\Theta_b - \Theta)\Theta_i \, \mathrm{d}\mathbf{x}. \tag{4.2}$$

From the symmetry of both bilinear forms, the following equality holds true:

$$\int_\Omega \sigma\varphi \mathrm{Re}\{E \cdot \overline{E}_i\} \, \mathrm{d}\mathbf{x} = 2\beta_2 \int_{\mathcal{T}} (\Theta^* - \Theta)\Theta_i \, \mathrm{d}\mathbf{x} + 2\beta_1 \int_{\mathcal{B}\setminus\mathcal{T}} (\Theta_b - \Theta)\Theta_i \, \mathrm{d}\mathbf{x}. \tag{4.3}$$

Therefore, equation (3.13) can be rewritten as

$$d_i = -\int_\Omega \sigma\varphi \mathrm{Re}\{E \cdot \overline{E}_i\} \, \mathrm{d}\mathbf{x}, \tag{4.4}$$

where φ is solution to the variational problem (2.10). Now, let us take $W = V$ in (3.7) and $W = E_i$ in (2.11) to obtain

$$\int_{\mathcal{D}} \left[\nabla \times E_i \cdot \nabla \times V - \varepsilon\mu\omega^2 E_i \cdot V\right] \mathrm{d}\mathbf{x} = \int_{\mathcal{D}} \nabla_{\mathbf{x}_i} \delta_\epsilon(\mathbf{x} - \mathbf{x}_i) \cdot V \, \mathrm{d}\mathbf{x}, \tag{4.5}$$

$$\int_{\mathcal{D}} \left[\nabla \times E_i \cdot \nabla \times V - \varepsilon\mu\omega^2 E_i \cdot V\right] \mathrm{d}\mathbf{x} = \int_\Omega \sigma\varphi \overline{E} \cdot E_i \, \mathrm{d}\mathbf{x}. \tag{4.6}$$

After comparing (4.5) with (4.6), we obtain the following important equality

$$\int_{\mathcal{D}} \nabla_{\mathbf{x}_i} \delta_\epsilon(\mathbf{x} - \mathbf{x}_i) \cdot V \, \mathrm{d}\mathbf{x} = \int_\Omega \sigma\varphi E \cdot \overline{E}_i \, \mathrm{d}\mathbf{x}. \tag{4.7}$$

By taking the real part on both sides of (4.7), equation (4.4) can be rewritten as

$$d_i = -\int_{\mathcal{D}} \nabla_{\mathbf{x}_i} \delta_\epsilon(\mathbf{x} - \mathbf{x}_i) \cdot \mathrm{Re}\{V\} \, \mathrm{d}\mathbf{x}, \tag{4.8}$$

where V is solution to the adjoint problem (2.11).

Now we have all elements to devise a gradient descent algorithm. The basic idea consists in using the first order gradient $\mathbf{d}$ as a descent direction by setting $\mathbf{q} = -\gamma\mathbf{d}$, with $\gamma > 0$. After disregarding the higher order terms from (3.10), we get

$$\mathcal{J}(\Theta_\delta) \approx \mathcal{J}(\Theta) - \gamma \|\mathbf{d}\|^2. \tag{4.9}$$

By enforcing $\mathcal{J}(\Theta_\delta) = 0$, we obtain

$$\gamma := \frac{\mathcal{J}(\Theta)}{\|\mathbf{d}\|^2}. \tag{4.10}$$

The quantity $\mathbf{q}$ can be updated as follows

$$\mathbf{q} \leftarrow \mathbf{q} - \gamma \mathbf{d}. \tag{4.11}$$

Then we use standard Armijo scheme to upgrade the step-size γ during the iterative process.

The resulting first order method written in pseudo-code format is summarized in Algorithm 1 where the parameters ϵ_J and ϵ_γ are user-defined stop criteria. They are related to the difference between the actual and the previous objective functional values and the step-size into the descent direction, respectively. In the algorithm, $\mathbf{q}^0$ and $\mathbf{q}^\star$ are used to denote the initial guess and the final value for the current vector $\mathbf{q}$.

Algorithm 1: Antenna design algorithm

Input: Ω, $\mathcal{B}$, $\mathcal{T}$, $\epsilon_J, \epsilon_\gamma$, $\mathbf{q}^0$
Output: $\mathbf{q}^\star$

```
1  begin
2      j ← 0;
3      compute the Maxwell non-perturbed problem (2.4);
4      compute the heat non-perturbed problem (2.2)
5      compute the objective functional (2.1);
6      J_old ← J;
7      J_new ← 1 + J_old;
8      γ evaluated as in (4.10);
9      j ← j + 1;
10     while γ > ε_γ and ‖J_new − J_old‖ > ε_J and j < 200 do
11         compute the heat adjoint equation (2.10);
12         compute the Maxwell adjoint equation (2.11);
13         compute the steepest descent direction d (4.8);
14         compute γ (4.10);
15         while J_new > J_old do
16             compute q according to (4.11);
17             execute lines 3 to 5;
18             J_new ← J;
19             γ ← γ/2;
20         end while
21     end while
22 end
```

5. Numerical Experiments

In this section, the numerical experiments are presented employing the outlined Algorithm 1 from the previous section. The goal is to selectively heat specific targets within a geometrical domain representing either homogeneous or heterogeneous medium.

Let Ω denote a cube with side length 50 cm, surrounded by a perfectly matched layer (PML), with a thickness of 10 cm. The object of interest, $\mathcal{B}$, represents a sphere with

a radius of 15 cm centered at $(0, 0, 0)$, simulating healthy mammary tissue, which is primarily composed of fat. Throughout our simulations, we enforce a heat boundary condition of $\Theta_\Gamma = 25^\circ$ for all scenarios.

The pointwise antennas are positioned around the body $\mathcal{B}$ within the domain Ω, as shown in Figure 2. They are strategically placed at each vertex and at the center of every faces of Ω, totaling 14 antennas (Figure 2(a)). Eventually, 4 more antennas are added to each face of the cube, leading to 38 antennas (Figure 2(b)). Throughout our experiments, we consistently set the weight parameter β to 0.5 for the objective functional defined in (2.1). Additionally, the body $\mathcal{B}$ is encased in deionized water [2, 24] during experimentation. In addition, the working frequency is set as 600 MHz. Finally, in all examples we set a uniform initial current $q_i = 10$ mA, for $i = 1, \cdots, N$, with $N = 14$ or $N = 38$, depending on the adopted antenna distribution from Figure 2.

The variational problems are solved by using finite element method. In particular, the heat equations (2.2) and (2.10) are discretized with tetrahedron P1 elements [7], whereas the Maxwell equations (2.4) and (2.11) are discretized with tetrahedron Nédélec elements [14]. The finite element meshes are produced by dividing the domain $\mathcal{D}$ in $70 \times 70 \times 70$ uniform voxels. Each resulting voxel is divided in 6 tetrahedrons, which leads to 357 911 nodes and 2 058 000 tetrahedrons. The parameter ϵ representing the aperture of the Gaussian function used to approximate the dipoles from (2.6) is given by the size of the smallest finite element. It is noteworthy that the experiments detailed in this section were implemented in *FreeFem++* version 4.13.

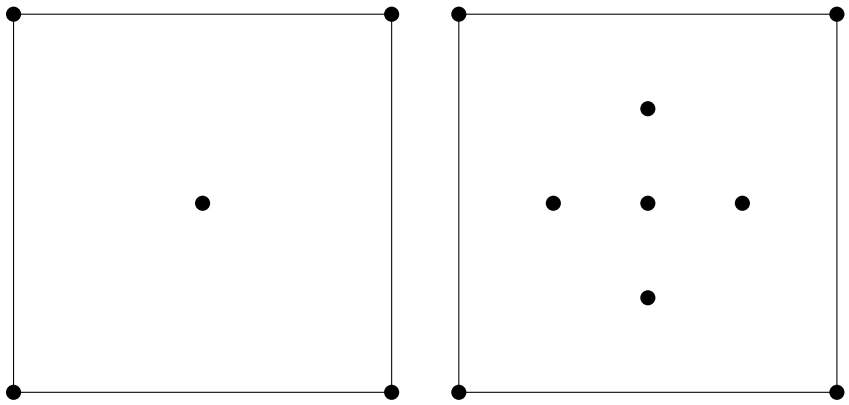

(a) 14 antennas (b) 38 antennas

FIGURE 2. Antenna distribution.

5.1. **Example 1 - Homogeneous Domain.** In this specific example, the domain is homogeneous where the tumor shares identical physical properties with the surrounding healthy tissue, essentially serving as a target for the algorithm. Here, the spherical target is centered at coordinate $(5, 5, 5)$ cm and having a radius of 6 cm. The difficulty arises from the absence of any heterogeneity in the material properties highlighting the target region, so that 14 antennas are insufficient to selectively heating the target. Therefore, in this particular example we use 38 antennas according to Figure 2(b). Figure 3 shows the cross section of Ω at $x = 5$ cm and Table 1 shows the used physical properties [2, 9, 24].

The algorithm stopped after reaching the maximum number of iterations set as 200, but with a negligible improvement on the temperature distribution during the last few iterations. The obtained results at the end of the iterative process are presented in Figures 4 and 5. Figure 4 shows the temperature distribution for cross sections yz, xz and xy. The region where the temperature exceeds 39°C is highlighted in Figure 5. Note that,

the method was able to heat the target. However, some hot-spot regions can be seen, nonetheless, considering the difficulty of this problem, the result is promising. Finally, the history of the iterative process is shown in Figure 5. At iteration 200, the current intensity values q_i ranged from -370.54 mA to 340.34 mA in signed values, and from 16.83 mA to 370.54 mA considering absolute value.

In the next examples, the target is physically characterized as a tumor, which is more vascularized and, for that reason, it becomes an "easier" target for the method due to the higher concentration of metals in the blood. Therefore, in the subsequent experiments, we use 14 antennas according to Figure 2(a), since now the use of more antennas do not produce significant improvement in the temperature distribution.

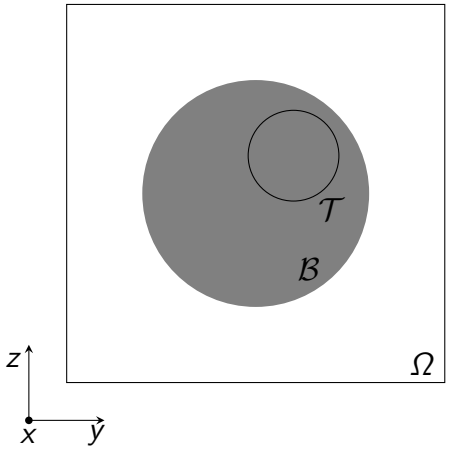

FIGURE 3. Example 1. Cross section of Ω at $x = 5$ cm: In gray the healthy tissue $\mathcal{B}$ and highlighted target $\mathcal{T}$.

TABLE 1. Example 1: Experiment physical properties.

Domain	K [W m^{-1} K^{-1}]	w [kg m^{-3} s^{-1}]	σ [S m^{-1}]	ϵ_r [F m^{-1}]
PML	1.0	0.0	1.0	1.0
Water	0.5	0.0	1.0×10^{-4}	76.5
Mammary	0.22	1.1	0.14	17

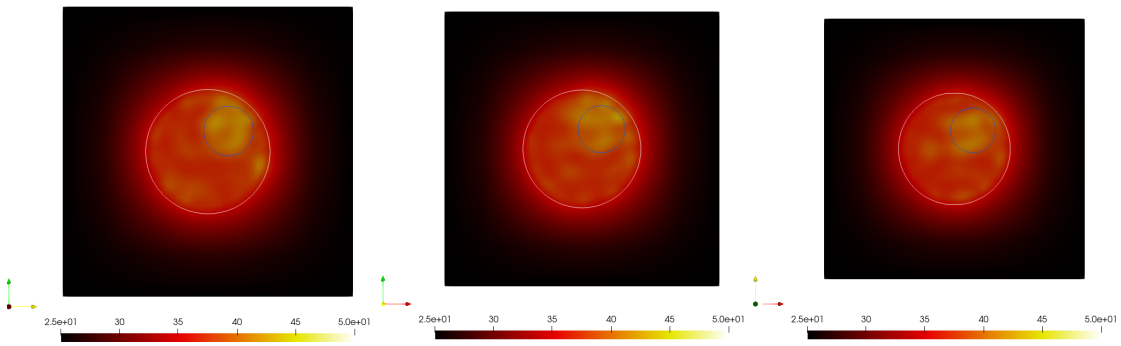

(a) (b) (c)

FIGURE 4. Example 1. Temperature distribution after 200 iterations for cross sections: yz-plane at $x = 5$ cm (a), xz-plane at $y = 5$ cm (b) and xy-plane at $z = 5$ cm (c).

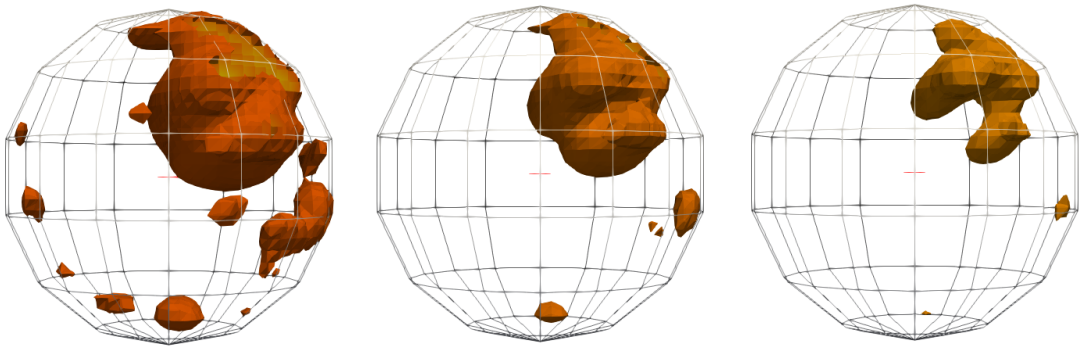

(a) (b) (c)

FIGURE 5. Example 1: The image shows the region where the temperature is above 39 (a), 40 (b) and 41 (c) Celsius degrees, respectively.

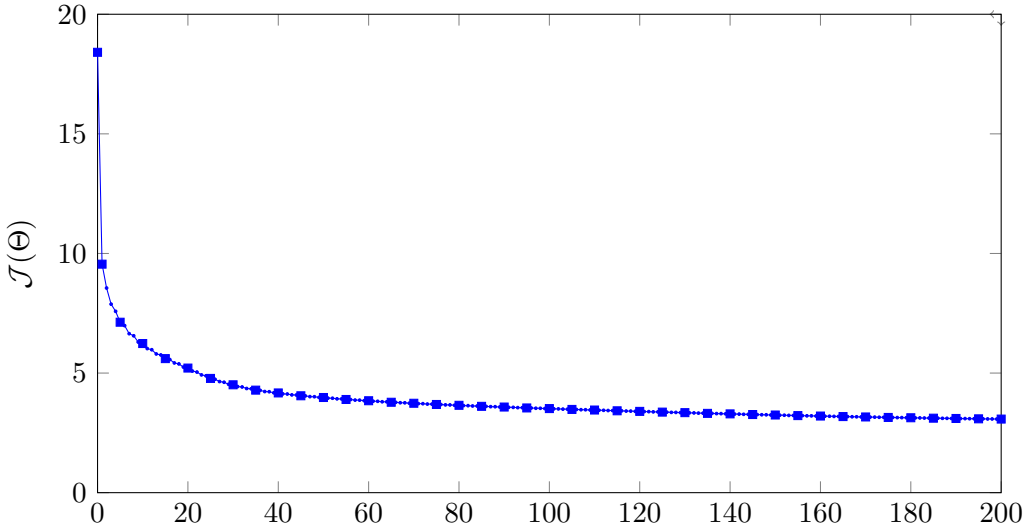

FIGURE 6. Example 1: History of the objective function during the iterative process.

5.2. **Example 2 - Non Homogeneous Domain.** For the examples of this section, differently of the previous one, the targets will be treated as tumors, possessing physical properties distinct from those of the adjacent healthy tissue. The specific physical properties for the tumors are detailed in Table 2 from [2, 9], while the remaining physical properties stay consistent with those utilized in the previous example, as shown in Table 1. Here, only 14 antennas according to Figure 2(a) are used.

TABLE 2. Example 2: Tumor physical properties.

Domain	K [W m^{-1} K^{-1}]	w [kg m^{-3} s^{-1}]	σ [S m^{-1}]	ϵ_r [F m^{-1}]
Tumor	0.56	1.8	0.95	57.4

5.2.1. *One tumor.* In this example, we employ the same setup as in Example 1 (Section 5.1), with the distinction that the target is characterized as a tumor. See the physical properties values in Table 2.

The algorithm converges after 174 iterations. Figures 7(a) and 7(b) provide a three-dimensional view of the temperature distribution for the problem, showing the intersection

between planes $x = 5$, $y = 5$ and $z = 5$, respectively for the initial guess and for the final result. Note that in Figure 7(a), the tumor $\mathcal{T}$ is almost at the same temperature as the rest of the body $\mathcal{B}$.

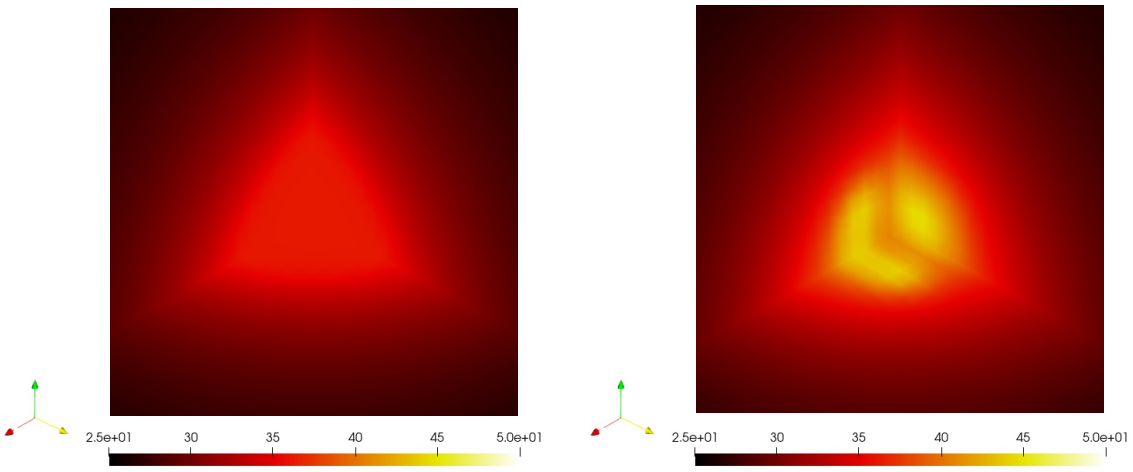

(a) (b)

FIGURE 7. Example 2 (one tumor): Initial (a) and final (b) temperature distributions in intersection between planes $x = 5$, $y = 5$ and $z = 5$, centered in $(5, 5, 5)$.

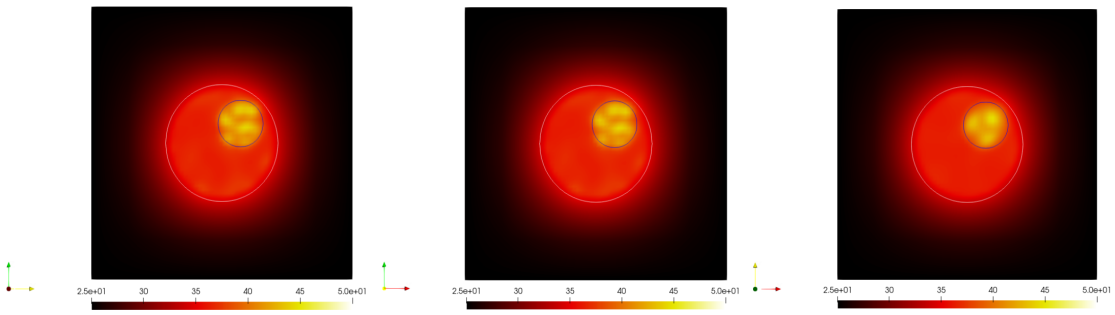

(a) (b) (c)

FIGURE 8. Example 2 (one tumor): Temperature distribution after 174 iterations for cross sections yz-plane at $x = 5$ cm (a), xz-plane at $y = 5$ cm (b) and xy-plane at $z = 5$ cm (c).

In Figure 8, sections of all axes are displayed, demonstrating that the tumor was heated as intended, while the rest of the body remained at a temperature close to 36 °C. In Figure 9, the region of the domain where the temperature exceeds 39 °C is highlighted. Notably, only the tumor region (marked with a gray grid) shows temperatures above this threshold. Figure 10 presents the history of the objective functional during the iterative process up to iteration 174. The final current intensity values q_i ranged from -134.39 mA to 153.66 mA in signed values, and from 1.01 mA to 153.66 mA when considering absolute values.

In Figure 11, the intensity and signal of each antenna are displayed. The radius of each circle is proportional to the current intensity, normalized by the maximum intensity, where dot ($\bullet$) and cross ($\times$) represent positive and negative values, respectively. A cube

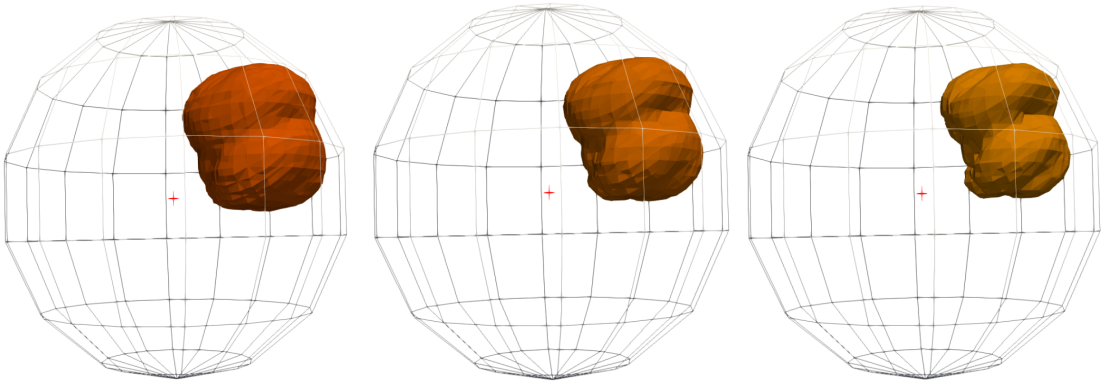

(a) (b) (c)

FIGURE 9. Example 2 (one tumor): The image shows the region where the temperature is above 39 (a), 40 (b) and 41 (c) Celsius degrees, respectively.

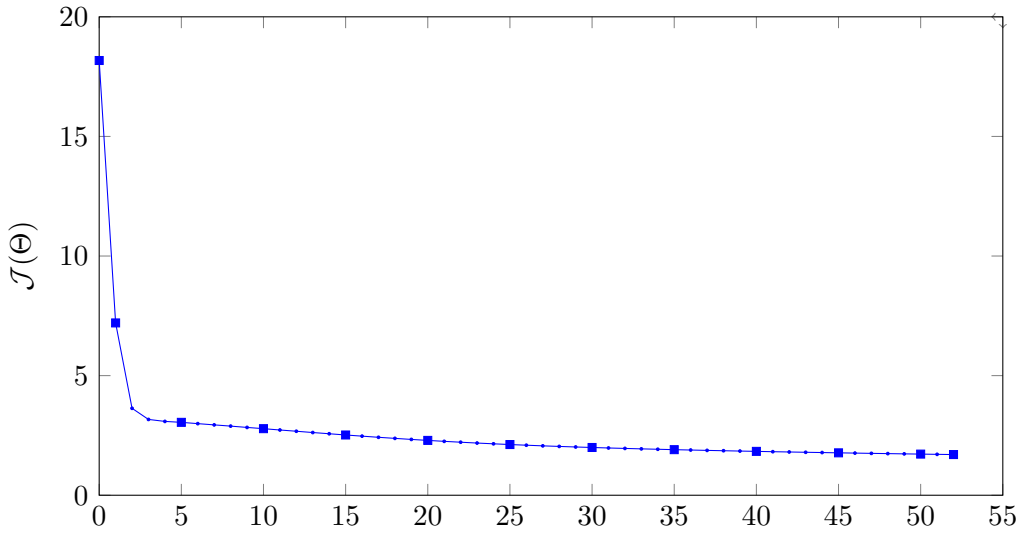

FIGURE 10. Example 2 (one tumor): History of the objective functional during the iterative process.

layout was used to represent the Ω domain. Note that, some antennas have minimum contribution. For the convenience of interested readers, the final current values are reported in Table 3.

TABLE 3. Example 2 (one tumor): Final current values [A] at the vertices (left) and at the faces (right) of the cube Ω.

$\mathbf{x}_i$	$q_i^\star$
$(-25, -25, -25)$	$+0.079863$
$(-25, -25, \ \ 25)$	-0.002135
$(-25, \ \ 25, -25)$	$+0.142014$
$(-25, \ \ 25, \ \ 25)$	$+0.001943$
$(\ \ 25, -25, -25)$	$+0.140852$
$(\ \ 25, -25, \ \ 25)$	$+0.002671$
$(\ \ 25, \ \ 25, -25)$	-0.023670
$(\ \ 25, \ \ 25, \ \ 25)$	-0.026528

$\mathbf{x}_i$	$q_i^\star$
$(\ \ 0, \ \ 0, \ \ 25)$	-0.148684
$(\ \ 0, \ \ 0, -25)$	$+0.160415$
$(-25, \ \ 0, \ \ 0)$	$+0.013750$
$(\ \ 25, \ \ 0, \ \ 0)$	$+0.015726$
$(\ \ 0, \ \ 25, \ \ 0)$	$+0.015411$
$(\ \ 0, -25, \ \ 0)$	$+0.012939$

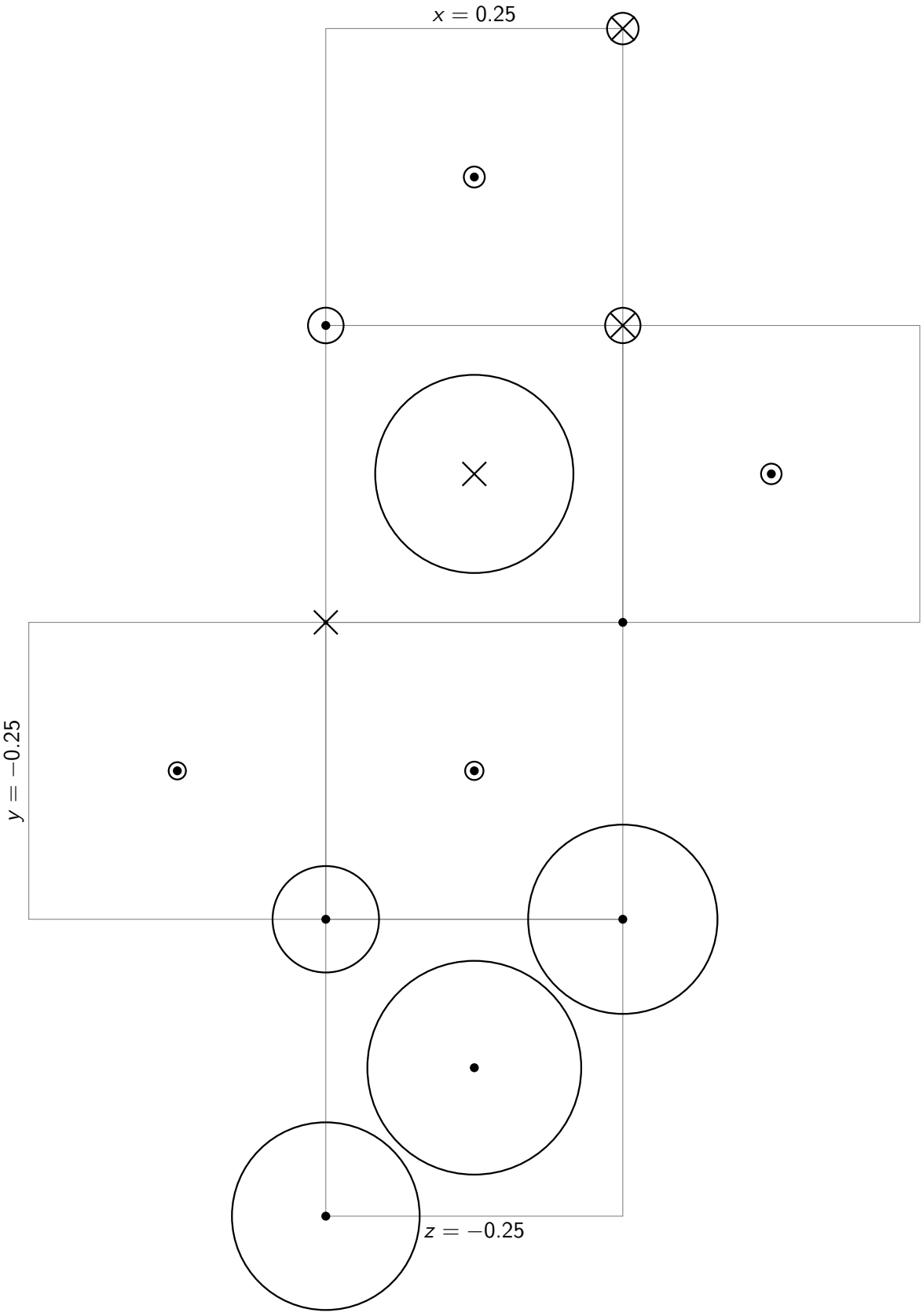

FIGURE 11. Example 2 (one tumor): Antennas's proportional intensities in a cube planning view. Positive and negative intensities are represented by dot (•) center and cross (×) center, respectively.

5.2.2. *Two tumors.* For this example, we have two spherical tumors positioned at coordinates $(6.5, 6.5, 6.5)$ and $(-6.5, -6.5, -6.5)$, both with radius of 5 cm. See Sketch in Figure 12. The physical properties values are reported in Tables 1 and 2.

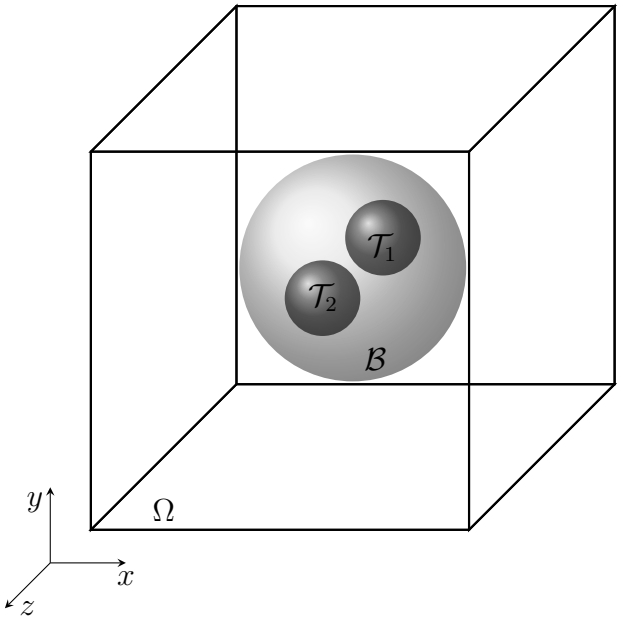

FIGURE 12. Example 2 (two tumors): In gray the healthy tissue $\mathcal{B}$ and in black the tumors $\mathcal{T}_1$ e $\mathcal{T}_2$

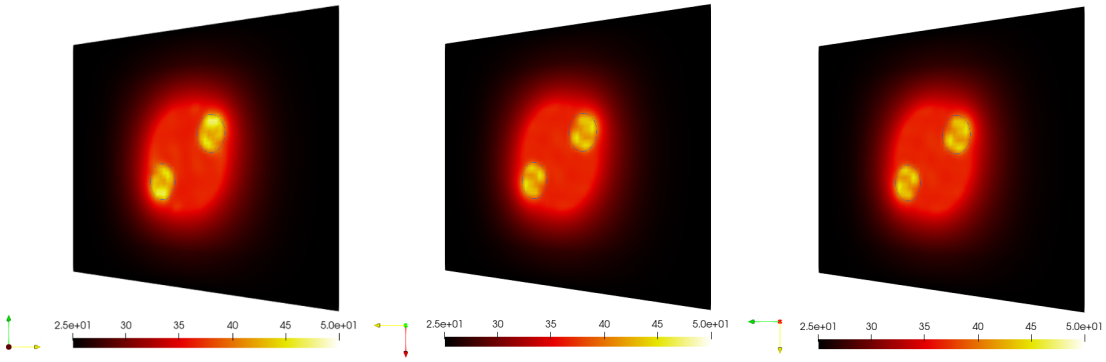

(a) (b) (c)

FIGURE 13. Example 2 (two tumors). Temperature distribution after 62 iterations for cross sections $y + z = -6.5$ cm, $x = 6.5$ cm (a), $x = z = -6.5$ cm, $y = 6.5$ cm (b) and $x + y = -6.5$ cm, $z = 5$ cm (c).

The algorithm converges after 62 iterations. In Figure 13, sections of all axes are presented for both tumors, indicating that the tumors were heated as intended while the rest of the body maintained a temperature of approximately 36 °C. However, it is important to note that the method encountered difficulties in effectively heating only the tumors, which resulted in the surrounding area also being heated. The region of the domain where the temperature exceeds 39 °C is highlighted in Figure 14. Figure 15 presents the history of the objective functional during the iterative process up to 62 iterations.

For a better representation of the antennas, we again use a flattened cube to proportionally display the current intensity in each antenna. Now, the current intensity values

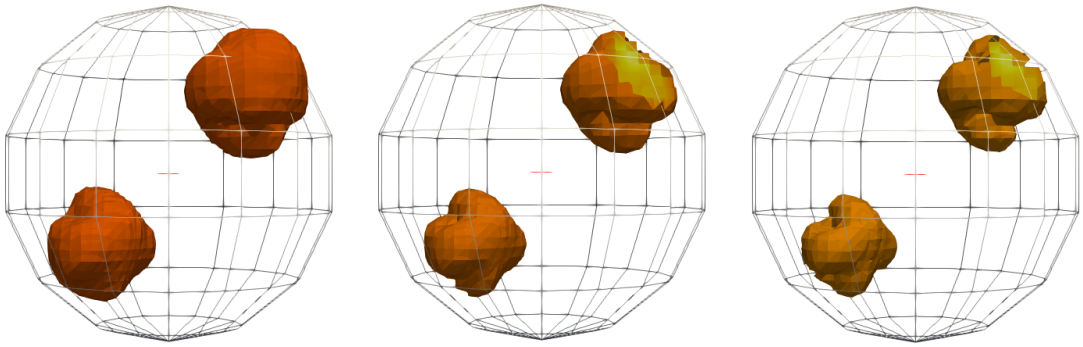

(a) (b) (c)

FIGURE 14. Example 2 (two tumors): The image shows the region where the temperature is above 39 (a), 40 (b) and 41 (c) Celsius degrees, respectively.

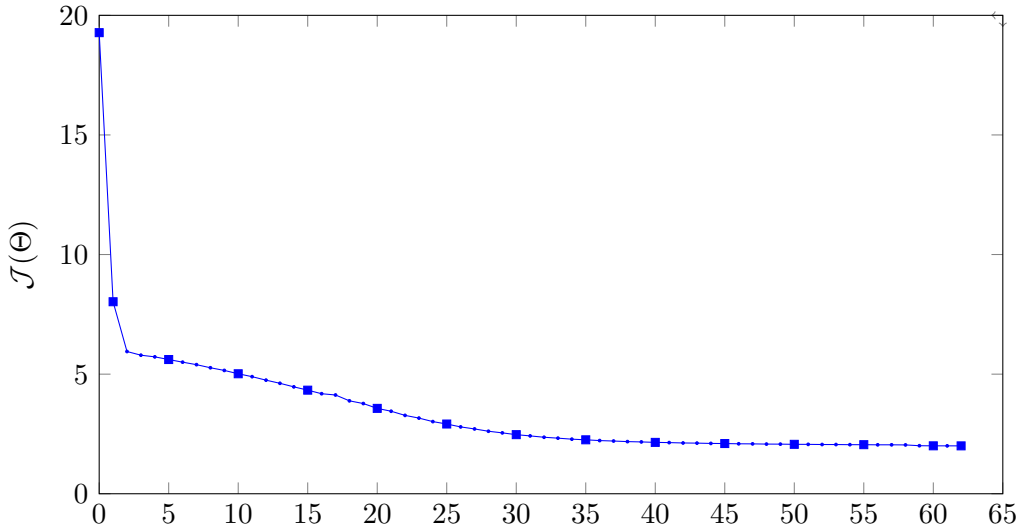

FIGURE 15. Example 2 (two tumors): History of the objective functional during the iterative process.

q_i ranged from -642.45 mA to 447.97 mA in signed values and from 156.26 mA to 642.45 mA when considering absolute values. Unlike the previous case, all 14 antennas made a significant contribution, each with at least 24% of the highest intensity.

6. Conclusion

In this work a novel pointwise antennas design for hyperthermia treatment into three spatial dimensions has been proposed. The forward problem was modeled by the variational forms of heat equation for living tissues coupled with Maxwell's equation. We utilize concepts of the topological derivative and adjoint sensitivity method to devise an optimization algorithm where the output is the optimal current values to pass through the antennas defined as dipoles, so that a given target or tumor was selectively heated.

A set of examples was presented with the aim of showing how the proposed method works. In a first example, we considered a completely homogeneous body $\mathcal{B}$, so that the problem becomes more challenging. Due to this, 38 antennas were used, positioned on

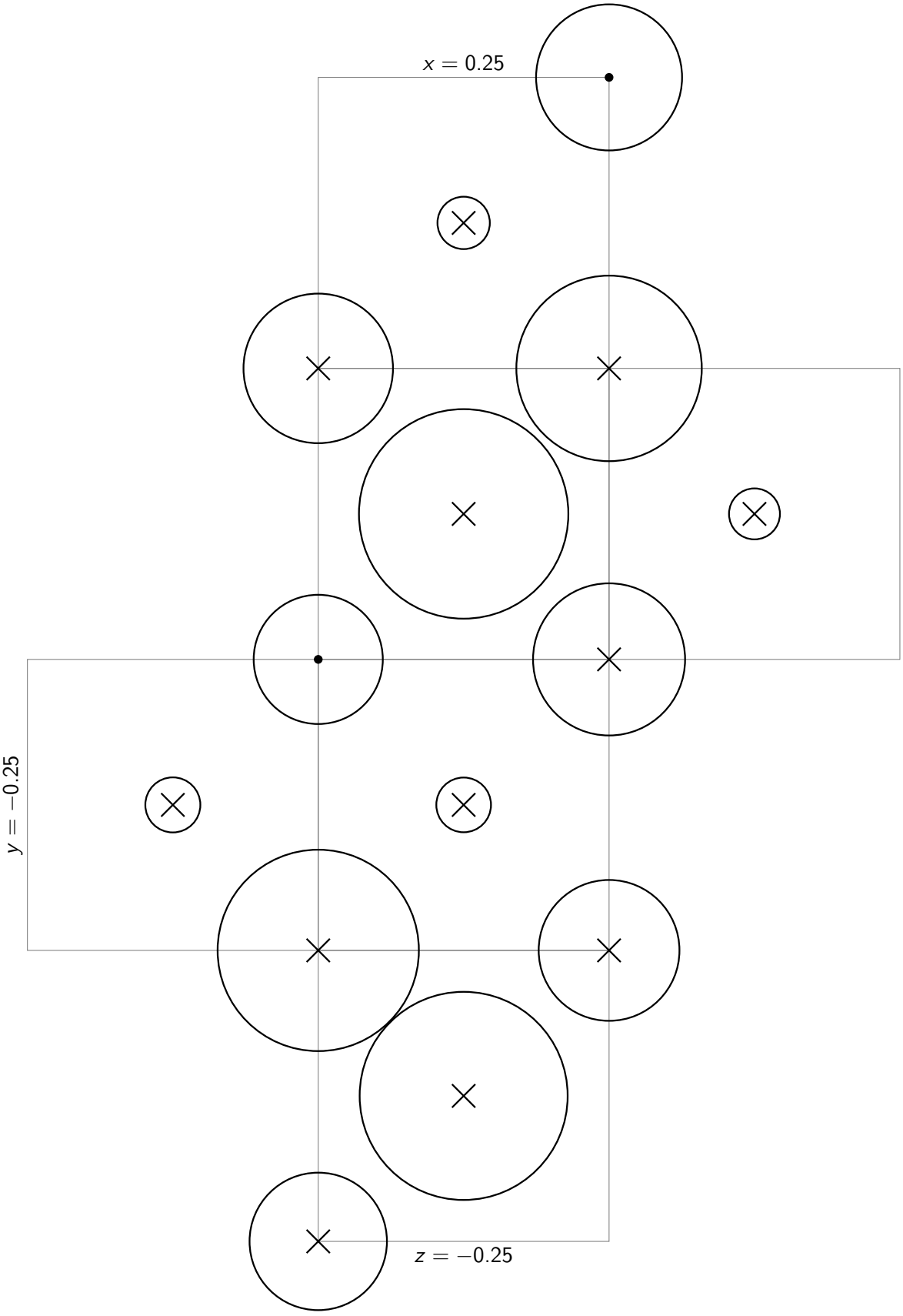

FIGURE 16. Example 2 (two tumors): Antennas's proportional intensities in a cube planning view. Positive and negative intensities are represented by dot (•) center and cross (×) center, respectively.

the faces and vertices of the domain Ω represented by a cube, as shown in Figure 2. The results obtained were satisfactory considering the difficulties of the problem.

In the following examples, we characterize the target as a tumor. The method was able to selectively heat one or two tumors at the same time. This ensures that the patient will not have burns in regions of healthy tissue even in the case of disjoint regions $\mathcal{T}$. It is worth mentioning that none of the experiments used contrast agents to highlight the tumor. The method relied only on the increased vascularization of tumor, leading to a fully noninvasive procedure which improves the possibility to use these treatments in patients who have allergy to the contrast, for instance.

Acknowledgements

This research was partly supported by CNPq (Brazilian Research Council), CAPES (Brazilian Higher Education Staff Training Agency) and FAPERJ (Research Foundation of the State of Rio de Janeiro). The support is gratefully acknowledged.

References

[1] K. Aki and P.G. Richards. *Quantitative Seismology*. University Science Books, Sausalito, California, 2009.

[2] A. A. S. Amad, A. F. D. Loula, and A. A. Novotny. A new method for topology design of electromagnetic antennas in hyperthermia therapy. *Applied Mathematical Modelling*, 42:209–222, 2017.

[3] D. T. Debela andS. G. Y. Muzazu, K. D. Heraro, M. T. Ndalama, B. W. Mesele, D. C. Haile, S. K. Kitui, and T. Manyazewal. New approaches and procedures for cancer treatment: Current perspectives. *SAGE open medicine*, 9:20503121211034366, 2021.

[4] J.J. Bosque, G.F. Calvo, and M. Cruz Navarro. Modelling the effect of vascular status on tumour evolution and outcome after thermal therapy. *Applied Mathematical Modelling*, 110:207–240, 2022.

[5] G. Danaei, S. Vander Hoorn, A. D. Lopez, C. J. L. Murray, M. Ezzati, Comparative Risk Assessment collaborating group (Cancers, and others). Causes of cancer in the world: comparative risk assessment of nine behavioural and environmental risk factors. *The Lancet*, 366(9499):1784–1793, 2005.

[6] G. Hegyi, G. P. Szigeti, and A. Szász. Hyperthermia versus oncothermia: cellular effects in complementary cancer therapy. *Evidence-Based Complementary and Alternative Medicine*, 2013, 2013.

[7] T. J. R. Hughes. *The finite element method: linear static and dynamic finite element analysis*. General Publishing Company, 2000.

[8] N.A. Jaffar, N. Buniyamin, and K. Lias. An overview of available metamaterial-based antenna for non-invasive hyperthermia cancer treatment. *Indonesian Journal of Electrical Engineering and Computer Science*, 14(2):697–705, 2019.

[9] W.T. Joines, Y. Zhang, C. Li, and R.L. Jirtle. The measured electrical properties of normal and malignant human tissues from 50 to 900 MHz. *Medical physics*, 21(4):547–550, 1994.

[10] E. Jones, D. Thrall, M. W. Dewhirst, and Z. Vujaskovic. Prospective thermal dosimetry: the key to hyperthermia's future. *International Journal of Hyperthermia*, 22(3):247–253, 2006.

[11] A.N. Khan, Y.O. Cha, H. Giddens, and Y. Hao. Recent advances in organ specific wireless bioelectronic devices: Perspective on biotelemetry and power transfer using antenna systems. *Engineering*, 11:27–41, 2022.

[12] T. J. Machado, J. S. Angelo, and A. A. Novotny. A new one-shot pointwise source reconstruction method. *Mathematical Methods in the Applied Sciences*, 40(15):1367–1381, 2017.
[13] R. Mattoso and A.A. Novotny. Pointwise antennas design in hyperthermia therapy. *Applied Mathematical Modelling*, 89:89–104, 2021.
[14] P. Monk. *Finite Element Methods for Maxwell's Equations*. Numerical Mathematics and Scientific Computation. Oxford University Press, Oxford, UK, 2003.
[15] H. R. Moyer and K. A. Delman. The role of hyperthermia in optimizing tumor response to regional therapy. *International Journal of Hyperthermia*, 24(3):251–261, 2008.
[16] A. A. Novotny and J. Sokołowski. *Topological derivatives in shape optimization*. Interaction of Mechanics and Mathematics. Springer-Verlag, Berlin, Heidelberg, 2013.
[17] H. H. Pennes. Analysis of tissue and arterial blood temperatures in the resting human forearm. *Journal of Applied Physiology*, 1(2):93–123, 8 1948.
[18] S. Pongpakpien, N. Shaichompu, , and Ph. Rattanadecho. Targeted therapy in liver tumor: Study on nanoparticle assisted with porous liver model. *Science and Technology Asia*, 26(2):87–98, 2021.
[19] Y. Tang, T. Jin, and R.C.C. Flesch. Effect of mass transfer and diffusion of nanofluid on the thermal ablation of malignant cells during magnetic hyperthermia. *Applied Mathematical Modelling*, 83:122–135, 2020.
[20] Y. Tang, J. Zou, R.C.C. Flesch, and T. Jin. Backflow modeling in nanofluid infusion and analysis of its effects on heat induced damage during magnetic hyperthermia. *Applied Mathematical Modelling*, 140:583–600, 2023.
[21] N. Uddin and I. Elshafiey. Efficient energy localization for hybrid wideband hyperthermia treatment system. *International Journal of RF and Microwave Computer-Aided Engineering*, 28(3), 2018.
[22] WHO - World Health Organization. Lung cancer, 2023.
[23] World Health Organization. Cancer incidence and mortality data. Technical report, International Agency for Reaserach on Cancer, 2022.
[24] L. Wu, R.J. McGough, O. A. Arabe, and T. V. Samulski. An RF phased array applicator designed for hyperthermia breast cancer treatments. *Physics in Medicine and Biology*, 51(1):1–20, dec 2005.
[25] P. Wust, B. Hildebrandt, G. Sreenivasa, B. Rau, J. Gellermann, H. Riess, R. Felix, and P.M. Schlag. Hyperthermia in combined treatment of cancer. *The Lancet Oncology*, 3(8):487–497, 2002.

(R. Mattoso) Laboratório Nacional de Computação Científica LNCC/MCTI, Coordenação de Métodos Matemáticos e Computacionais, Av. Getúlio Vargas 333, 25651-075 Petrópolis - RJ, Brasil
Email address: rmattoso@posgrad.lncc.br

(A.A. Novotny) Laboratório Nacional de Computação Científica LNCC/MCTI, Coordenação de Métodos Matemáticos e Computacionais, Av. Getúlio Vargas 333, 25651-075 Petrópolis - RJ, Brasil
Email address: novotny@lncc.br

(Ravi Prakash) Departamento de Matemática, Facultad de Ciencias Físicas y Matemáticas, Universidad de Concepción, Avenida Esteban Iturra s/n, Bairro Universitario, Casilla 160 C, Concepción, Chile.
Email address: rprakash@udec.cl